Observation of the Anisotropic Photoinduced Magnetization Effect in Co−Fe Prussian Blue Thin Films Fabricated by Using Clay Langmuir−Blodgett Films as a Template

ARTICLE *in* JOURNAL OF THE AMERICAN CHEMICAL SOCIETY · DECEMBER 2005

Impact Factor: 12.11 · DOI: 10.1021/ja053131e · Source: PubMed

4 AUTHORS, INCLUDING:

Takashi Yamamoto
Keio University
24 PUBLICATIONS **330** CITATIONS

SEE PROFILE

J|A|C|S
ARTICLES
Published on Web 11/02/2005

Observation of the Anisotropic Photoinduced Magnetization Effect in Co−Fe Prussian Blue Thin Films Fabricated by Using Clay Langmuir−Blodgett Films as a Template

Takashi Yamamoto,[†] Yasushi Umemura,[‡] Osamu Sato,[§] and Yasuaki Einaga*,[†]

Contribution from the Department of Chemistry, Faculty of Science and Technology, Keio University, 3-14-1 Hiyoshi, Yokohama 223-8522, Japan, Department of Applied Chemistry, National Defense Academy, 1-10-20 Hashirimizu, Yokosuka 239-8686, Japan, and Institute for Materials Chemistry and Engineering, Kyushu University, 6-1 Kasuga-Kouen, Kasuga 816-8580, Japan

Received May 13, 2005; E-mail: einaga@chem.keio.ac.jp

Abstract: Thin films of cobalt−iron cyanide (Co−Fe Prussian blue) have been fabricated by means of the modified Langmuir−Blodgett (LB) method using a smectite clay mineral (montmorillonite). In this combined method, clay LB films play a template role in the formation of the Co−Fe Prussian blue thin layer. The films were revealed to possess a well-organized structure not only in perpendicular directions to the film surface but also in parallel directions to the film surface. The photoinduced electron transfer from the iron ion to the cobalt through the bridging cyanide in the films occurred at low temperature (8 K), similar to that in the bulk Co−Fe Prussian blue. The films clearly exhibited magnetic anisotropy with regards to the direction of the applied magnetic field. Moreover, the photoinduced magnetization effect in the films was also found to be anisotropic.

Introduction

Numerous solid-state metal cyanides are well-known, and especially in the field of the molecular magnetism, they have been paid much attention because of the cyanide ligand's ability to efficiently mediate the magnetic exchange interaction. Actually, these cyanide-bridged compounds form different network structures: one-dimensional (chain),[1] two-dimensional (sheet),[2] and three-dimensional (cubic).[3] Among them, Prussian blue and its analogues, with the general formula $A_{2x}M'^{II}_{(1.5-x)}[M^{III}(CN)_6]$ ($x = 0-1$; A = alkali metal ion; M^{II}, M^{III} = transition metal ions), have been extensively investigated due to their fascinating magnetic properties, such as high Curie temperature (T_C),[4] photoinduced magnetization[5] and magnetic pole inversion,[6] humidity response,[6b] electrotuning,[7] pressure tuning,[8] and so on. Thus, the Prussian blue family exhibits not only spontaneous magnetization below T_C but also responds to external stimuli such as light, humidity, and pressure. Although it is required to fabricate its organized thin films in the application for devices, magnetic properties in these compounds have been mainly explored in the bulk. In general, up to now, thin films have

[†] Keio University.
[‡] National Defense Academy.
[§] Kyushu University.

(1) (a) Ohba, M.; Maruono, N.; Okawa, H.; Enoki, T.; Latour, J. M. *J. Am. Chem. Soc.* **1994**, *116*, 11566. (b) Miyasaka, H.; Matsumoto, N.; Okawa, H.; Re, N.; Gallo, E.; Floriani, C. *J. Am. Chem. Soc.* **1996**, *118*, 981. (c) Kou, H.-Z.; Liao, D.-Z.; Cheng, P.; Jiang, Z.-H.; Yan, S.-P.; Wang, G.-L.; Yao, X.-K.; Wang, H.-G. *J. Chem. Soc., Dalton Trans.* **1997**, 1503. (d) Langenberg, K. V.; Batten, S. R.; Berry, K. J.; Hockless, D. C. R.; Moubaraki, B.; Murray, K. S. *Inorg. Chem.* **1997**, *36*, 5006. (e) Miyasaka, H.; Ieda, H.; Matsumoto, N.; Re, N.; Crescenzi, R.; Floriani, C *Inorg. Chem.* **1998**, *37*, 255. (f) Ohba, M.; Usuki, N.; Fukita, N.; Okawa, H. *Inorg. Chem.* **1998**, *37*, 3349.

(2) (a) Miyasaka, H.; Matsumoto, N.; Okawa, H.; Re, N.; Gallo, E.; Floriani, C. *Angew. Chem. Int. Ed.* **1995**, *34*, 1446. (b) Ohba, M.; Fukita, N.; Okawa, H.; Hashimoto, Y. *J. Am. Chem. Soc.* **1997**, *119*, 1011. (c) Miyasaka, H.; Matsumoto, N.; Re, N.; Gallo, E.; Floriani, C. *Inorg. Chem.* **1997**, *36*, 670. (d) Ohba, M.; Okawa, H. *Coord. Chem. Rev.* **2000**, *198*, 313. (e) Miyasaka, H.; Ieda, H.; Matsumoto, N.; Sugiura, K.; Yamashita, M. *Inorg. Chem.* **2003**, *42*, 3509.

(3) (a) Herren, F.; Fischer, P.; Ludi, A.; Hälg, W. *Inorg. Chem.* **1980**, *19*, 956. (b) Lu, J.; Harrison, W. T. A.; Jacobson, A. J. *Angew. Chem. Int. Ed.* **1995**, *34*, 2557. (c) El Fallah, S. E.; Rentschler, E.; Caneschi, A.; Sessoli, R.; Gatteschi, D. *Angew. Chem. Int. Ed.* **1996**, *35*, 1947. (d) Ohba, M.; Usuki, N.; Fukita, N.; Okawa, H. *Angew. Chem. Int. Ed.* **1999**, *38*, 1795. (e) Li, G.-M.; Akitsu, T.; Sato, O.; Einaga, Y. *J. Am. Chem. Soc.* **2003**, *125*, 12396. (f) Hozumi, T.; Hashimoto, K.; Ohkoshi, S. *J. Am. Chem. Soc.* **2005**, *127*, 3864.

(4) (a) Ferlay, S.; Mallah, T.; Ouahes, R.; Veillet, P.; Verdaguer, M. *Nature* **1995**, *378*, 701. (b) Entley, W. R.; Girolami, G. S. *Science* **1995**, *268*, 397. (c) Dujardin, E.; Ferlay, S.; Phan, X.; Desplanches, C.; Moulin, C. C. D.; Sainctavit, P.; Baudelet, F.; Dartyge, E. Veillet, P.; Verdaguer, M. *J. Am. Chem. Soc.* **1998**, *120*, 11347. (d) Ferlay, S.; Mallah, T.; Ouahes, R.; Veillet, P.; Verdaguer, M. *Inorg. Chem.* **1999**, *38*, 229. (e) Hatlevik, O.; Buschmann, W. E.; Zhang, J.; Manson, J. L.; Miller, J. S. *Adv. Mater.* **1999**, *11*, 914. (f) Holmes, S. D.; Girolami, G. *J. Am. Chem. Soc.* **1999**, *121*, 5593.

(5) (a) Sato, O.; Iyoda, T.; Fujishima, A.; Hashimoto, K. *Science* **1996**, *272*, 704. (b) Sato, O.; Einaga, Y.; Fujishima, A.; Hashimoto, K. *Inorg. Chem.* **1999**, *38*, 4405. (c) Bleuzen, A.; Lomenech, C.; Escax, V.; Villain, F.; Varret, F.; Moulin, C. C. D.; Verdaguer, M. *J. Am. Chem. Soc.* **2000**, *122*, 6648. (d) Escax, V.; Bleuzen, A.; Cartier dit Moulin, C.; Villain, F.; Goujon, A.; Varret, F.; Verdaguer, M. *J. Am. Chem. Soc.* **2001**, *123*, 12536. (e) Shimamoto, N.; Ohkoshi, S.; Sato, O.; Hashimoto, K. *Inorg. Chem.* **2002**, *41*, 678.

(6) (a) Ohkoshi, S.; Hashimoto, K. *J. Am. Chem. Soc.* **1999**, *121*, 10591. (b) Ohkoshi, S.; Arai, K.; Sato, Y.; Hashimoto, K. *Nat. Mater.* **2004**, *3*, 857.

(7) (a) Dostal, A.; Schröder, U.; Scholz, F. *Inorg. Chem.* **1995**, *34*, 1711. (b) Kulesza, P. J.; Malik, M. A.; Miecznikowski, K.; Wolkiewicz, A. *J. Electrochem. Soc.* **1996**, *143*, L10. (c) Sato, O.; Iyoda, T.; Fujishima, A.; Hashimoto, K. *Science* **1996**, *271*, 49.

(8) (a) Moritomo, Y.; Hanawa, M.; Ohishi, Y.; Kato, K.; Takata, M.; Kuriki, A.; Nishibori, E, Sakata, M.; Ohkoshi, S.; Tokoro, H.; Hashimoto, K. *Phys. Rev. B* **2003**, *68*, 144106. (b) Ksenofontov, V.; Levchenko, G.; Reiman, S.; Gütlich, P.; Bleuzen, A.; Escax, V.; Verdaguer, M. *Phys. Rev. B* **2003**, *68*, 024415. (c) Coronado, E.; Giménez-Lopéz, M. C.; Levchenko, G.; Romero, F. M.; Garcia-Baonza, V.; Milner, A.; Paz-Pasternak, M. *J. Am. Chem. Soc.* **2005**, *127*, 4580.

been mainly prepared by an electrochemical[9] or an ion-exchange method.[10] However, from the viewpoint of uniformity and orientation of the films, it seems inadequate to prepare thin films by the above methods.

The air−liquid interface is often used to direct assembly processes, and a careful understanding of these processes is now possible largely as a result of surface-sensitive characterization methods.[11] Traditional Langmuir monolayers can form two-dimensional molecular crystals[11,12] or can selectively bind molecules or ions from the subphase to produce multicomponent assemblies.[11,13] They are also used to induce the heterogeneous nucleation of three-dimensional crystals, where chemical or stereochemical features of the monolayer can direct the morphology, orientation, or chemical identity of the product crystals.[14] Langmuir−Blodgett (LB) films can be obtained by transferring the Langmuir monolayers onto the solid substrate. This method is called the LB method, in which the number of layers and their sequence can be controlled at the molecular level.[12a,15] On the basis of these features, metal cyanide extended networks, two-dimensional assemblies of Prussian blue, have also been fabricated as a part of LB films. Mingotaud et al. first reported the preparation of such LB films, in which Prussian blue related compounds were trapped within the amphiphilic bilayer.[16] They obtained Prussian blue LB films by spreading a positively charged lipid, dioctadecyldimethylammonium ion (DODA), on a very diluted colloidal dispersion of "soluble" Prussian blue (also its analogues).[16,17] In addition, recently, Culp et al. reported a different approach for preparing an extended metal cyanide network within the LB films.[18] In this approach, reaction of a Langmuir monolayer of the amphiphilic complex with metal ions from the subphase resulted in two-dimensional mixed-metal cyanide-bridged networks at the air−water interface. Confinement of the reactants to the air−water interface discriminates against the formation of higher-dimensionality products and directs the lateral propagation of the two-dimensional network. In addition to the above works, other methods have been reported in the fabrication of thin films of Prussian blue analogues.[19] Thus, there have been many examples that described the successful formation of Prussian blue (and also its analogues) thin films by cleverly making use of the air−water interface. However, with regard to Co−Fe Prussian blue (the Prussian blue analogue with Fe−CN−Co structures) that exhibits photoinduced magnetization effects, there have been only a few reports about the fabrication of thin films.[19a,b,20]

Our approach to the fabrication of Co−Fe Prussian blue thin films is to adopt the modified LB method using a clay mineral.[21] In detail, when amphiphilic cations are spread onto an aqueous suspension of a clay mineral in an LB trough, negatively charged clay single nanosheets in the suspension are adsorbed electrostatically onto the bottom of a floating monolayer of cations at the air−suspension interface. The outer surface of the transferred film is covered with a clay layer, and some exchangeable cations (Na^+) remain on the outer surface of the clay. Thus, when the outer surface of the film is dipped in a solution of a cationic compound, the cationic compound is adsorbed on the surface by an ion-exchange reaction to form a layer of the cations.[22] The hybrid films thus prepared are revealed to possess some remarkable features: (1) The layered structure of the film is quite stable due to the existence of the rigid clay layers. (2) Cationic compounds can be intercalated into the hybrid film by an ion-exchange reaction with the clay layer. (3) The cations in the adsorbed layer are sandwiched in a noncentrosymmetric fashion. Therefore, it would be effective to prepare thin films by this modified LB method. Actually, we have designed the photomagnetic hybrid films, consisting of an amphiphilic ammonium salt (cationic surfactants to form a floating monolayer at the interface), a smectite clay (montmorillonite; *Kunipia P*), and Co−Fe Prussian blue (a photomagnet).[20b] As expected, these hybrid films were revealed to be well-organized, and moreover, the photoinduced magnetization effect was observed, similarly to that in the bulk Co−Fe Prussian blue. Thus, the clay LB films composed of cationic amphiphiles and clay

(9) (a) Gao, Z.-Q.; Wang, G.-O.; Li, P.-B.; Zhao, Z. F. *Electrochim. Acta* **1991**, *36*, 147. (b) Joseph, J.; Gomathi, H.; Rao, G. P. *J. Electroanal. Chem.* **1991**, *304*, 263. (c) Sato, O.; Einaga, Y.; Iyoda, T.; Fujishima, A.; Hashimoto, K. *J. Electrochem. Soc.* **1997**, *144*, L11. (d) Ohkoshi, S.; Fujishima, A.; Hashimoto, K. *J. Am. Chem. Soc*. **1998**, *120*, 5349. (e) Ohkoshi, S.; Einaga, Y.; Fujishima, A.; Hashimoto, K. *J. Electroanal. Chem.* **1999**, *473*, 245. (f) Mizuno, M.; Ohkoshi, S.; Hashimoto, K. *Adv. Mater.* **2000**, *12*, 1955.

(10) (a) Tozawa, M.; Ohkoshi, S.; Kojima, N.; Hashimoto, K. *Chem. Commun.* **2003**, 1204. (b) Honda, K.; Hayashi, H. *J. Electrochem. Soc*. **1987**, *134*, 1330. (c) Honda, K.; Hayashi, H.; Chiba, K. *Chem. Lett.* **1988**, *17*, 191.

(11) Kuzmenko, I.; Rapaport, H.; Kjaer, K.; Als-Nielsen, J.; Weissbuch, I.; Lahav, M.; Leiserowitz, L. *Chem. Rev.* **2001**, *101*, 1659.

(12) (a) Ulman, A. *An Introduction to Ultrathin Organic Films: From Langmuir−Blodgett to Self-Assembly*; Academic Press: Boston, MA, 1991. (b) Jacquemain, D.; Wolf, S. G.; Leveiller, F.; Deutsch, M.; Kjaer, K.; Als-Nielsen, J.; Lahav, M.; Leiserowitz, L. *Angew. Chem. Int. Ed.* **1992**, *31*, 130. (c) Kaganer, V.; Möhwald, H.; Dutta, P. *Rev. Mod. Phys.* **1999**, *71*, 779.

(13) (a) Leveiller, F.; Bohm, C.; Jacquemain, D.; Möhwald, H.; Leiserowitz, L.; Kjaer, K.; Als-Nielsen, J. *Adv. Mater*. **1998**, *10*, 117. (b) Hensel, V.; Godt, A.; Popovitz-Biro, R.; Cohen, H.; Jensen, T. R.; Kjaer, K.; Weissbuch, I.; Lifshitz, E.; Lahav. M. *Chem. Eur. J*. **2002**, *8*, 1413.

(14) (a) Landau, E. M.; Levanon, M.; Leiserowitz, L.; Lahav, M.; Sagiv, J. *Nature* **1985**, *318*, 353. (b) Frostman, L. M.; Ward, M. D. *Langmuir* **1997**, *13*, 330. (c) Mann, S.; Heywood, B. R.; Rajam, S.; Walker, J. B. A.; Davey, R. J.; Birchall, J. D. *Adv. Mater.* **1990**, *2*, 257.

(15) (a) Gaines, G. L., Jr. *Insoluble Monolayers at Liquid−Gas Interfaces*; Wiley-Interscience: New York, 1966. (b) Kuhn, H.; Mobius, D.; Bucher, H. In *Physical Methods of Chemistry*; Weissberger, A., Rossiter, B., Eds.; John Wiley and Sons: 1972; Vol. 1, Part IIIB, pp 577−715. (c) Roberts, G. G. *Langmuir−Blodgett Films*; Plenum Press: New York, 1990. (d) Petty, M. C., *Langmuir−Blodgett Films. An Introduction*; Cambridge University Press: Cambridge, U.K., 1996.

(16) (a) Mingotaud, C.; Lafuente, C.; Amiell, J.; Delhaes, P. *Mol. Cryst. Liq. Cryst. Sci. Technol., Sect. A* **1999**, *335*, 1061. (b) Mingotaud, C.; Lafuente, C.; Amiell, J.; Delhaes, P. *Langmuir* **1999**, *15*, 289.

(17) (a) Lafuente, C.; Mingotaud, C.; Delhaes, P. *Chem. Phys. Lett.* **1999**, *302*, 523. (b) Romualudo-Torres, G.; Agricole, B.; Delhaes, P.; Mingotaud, C. *Chem. Mater* **2002**, *14*, 4012. (c) Romualudo-Torres, G.; Agricole, B.; Mingotaud, C.; Ravaine, S.; Delhaes, P. *Langmuir* **2003**, *19*, 4688.

(18) (a) Culp, J. T.; Park, J.-H.; Stratakis, D.; Meisel, M. W.; Talham, D. R. *J. Am. Chem. Soc.* **2002**, *124*, 10083. (b) Culp, J. T.; Park, J.-H.; Meisel, M. W.; Talham, D. R. *Polyhedron* **2003**, *22*, 2125. (c) Culp, J. T.; Park, J.-H.; Meisel, M. W.; Talham, D. R. *Inorg. Chem.* **2003**, *42*, 2842.

(19) (a) Choudhury, S.; Bagker, N.; Dey, G. K.; Subramanian, H.; Yakhmi, J. V. *Langmuir* **2002**, *18*, 7409. (b) Choudhury, S.; Dey, G. K.; Yakhmi, J. V. *J. Cryst. Growth* **2003**, *258*, 197. (c) Culp, J. T.; Park, J.-H.; Benitez, I. O.; Huh, Y.-D.; Meisel, M. W.; Talham, D. R. *Chem. Mater*. **2003**, *15*, 3431. (d) Bagker, N.; Ganguly, R.; Choudhury, S.; Hassan, P. A.; Sawant, S.; Yakhmi, J. V. *J. Mater. Chem.* **2004**, *14*, 1430.

(20) (a) Culp, J. T.; Park, J.-H.; Meisel, M. W.; Talham, D. R. *Polyhedron* **2003**, *22*, 3059. (b) Yamamoto, T.; Umemura, Y.; Sato, O.; Einaga, Y. *Chem. Lett.* **2004**, *33*, 500. (c) Park, J.-H.; Huh, Y.-D.; Čižmár, E.; Gamble, S. G.; Talham, D. R.; Meisel, M. W. *J. Magn. Magn. Mater.* **2004**, *272−276*, 1116. (d) Park, J.-H.; Čižmár, E.; Meisel, M. W.; Huh, Y.-D.; Frye, F.; Lane, S.; Talham, D. R. *Appl. Phys. Lett.* **2004**, *85*, 3797.

(21) (a) Tamura, K.; Setsuda, H.; Taniguchi, M.; Yamagishi, A. *Langmuir* **1999**, *15*, 6915. (b) Kawamata, J.; Ogata, Y.; Taniguchi, M.; Yamagishi, A.; Inoue, K. *Mol. Cryst. Liq. Cryst.* **2000**, *343*, 53. (c) Umemura, Y.; Yamagishi, A.; Schoonheydt, R. Persoons, A.; De Schryber, F. *Thin Solid Films* **2001**, *388*, 5. (d) Umemura, Y.; Yamagishi, A.; Schoonheydt, R.; Persoons, A.; De Schryber, F. *Langmuir* **2001**, *17*, 449. (e) Ras, R. H. A.; Németh, J.; Johnston, C. T.; Dékány, I.; Schoonheydt, R. A. *Phys. Chem. Chem. Phys.* **2004**, *6*, 5347. (f) Ras, R. H. A.; Németh, J.; Johnston, C. T.; DiMasi, E.; Dékány, I.; Schoonheydt, R. A. *Phys. Chem. Chem. Phys*. **2004**, *6*, 4174.

(22) (a) Umemura, Y.; Yamagishi, A.; Schoonheydt, R.; Persoons, A.; De Schryber, F. *J. Am. Chem. Soc.* **2002**, *124*, 992. (b) Umemura, Y. *J. Phys. Chem. B* **2002**, *106*, 11168. (c) Yamamoto, T.; Umemura, Y.; Sato, O.; Einaga, Y. *Chem. Mater*. **2004**, *16*, 1195.

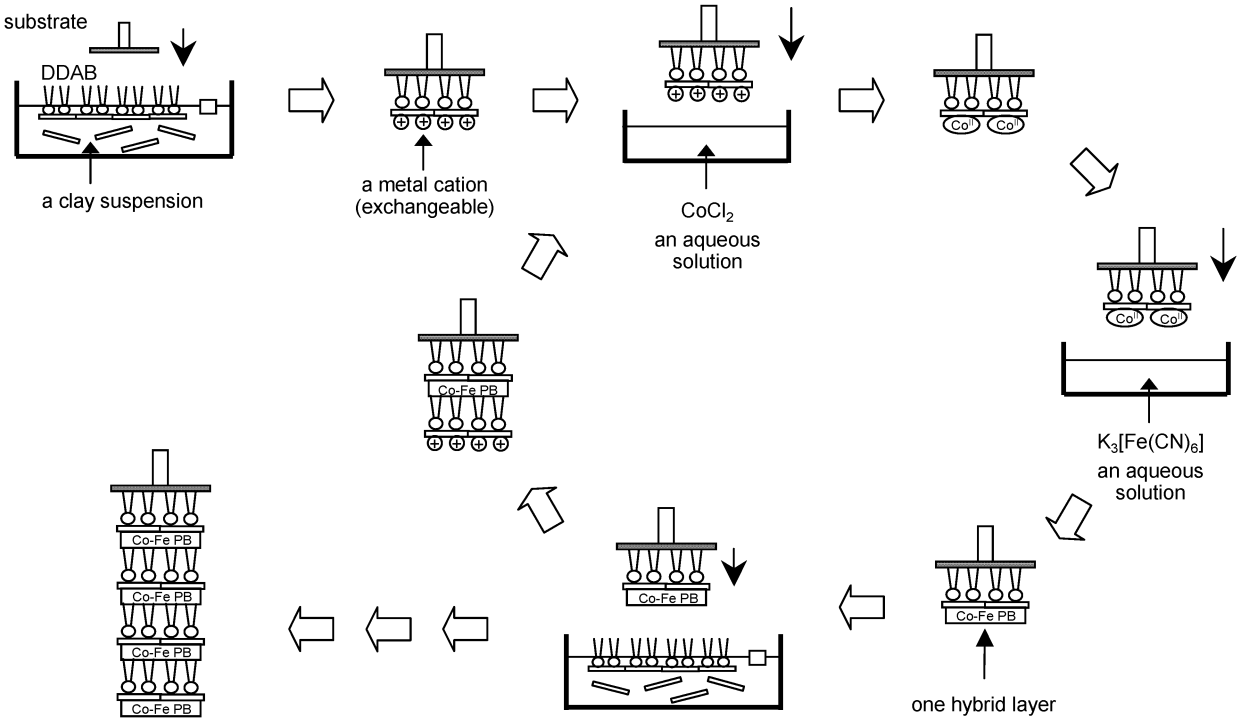

Figure 1. Schematic illustration of the film preparation method. Hybrid films are composed of DDAB, the clay single nanosheets, and Co−Fe Prussian blue.

minerals played a template role in the formation of the Co−Fe Prussian blue thin layer in this composite system.

As already mentioned above, there have been only a few reports about the successful fabrication of Co−Fe Prussian blue thin films.[19a,b,20] Among such works, Park et al. reported a very interesting phenomenon, so-called "anisotropic photoinduced magnetism". According to their results, upon light illumination at 5 K, the net magnetization of the film *increased* when the surface of the film was oriented parallel to the external magnetic field. On the other hand, when the surface of the film was perpendicular to the magnetic field, the net magnetization *decreased* upon illumination. They described that the anisotropic photoinduced magnetization effect in the film arises from the interplay between the low-dimensional nature of the system and the dipolar magnetic fields generated by the ferrimagnetic domain. This result offers a new insight to the magnetic property of Co−Fe Prussian blue and, in addition, provides a mechanism that may be useful in the future device application. We report herein an extended investigation for our previous photomagnetic hybrid films:[20b] the in-plane structure, spectroscopic studies, the magnetic anisotropy, and the photoinduced magnetization effect. As results, we observed an anisotropic photoinduced magnetization effect, which exhibits a different fashion from that observed by Park et al.[20d] In this work, the reaction of the cationic amphiphile and a clay mineral was examined by surface pressure−molecular area (π−A) isotherm measurements. The structure of the resulting hybrid films was confirmed by X-ray diffraction (XRD) and X-ray photoelectron spectroscopy (XPS). The photoinduced electron-transfer process was monitored by FT-IR absorption spectroscopy (FT-IR), and magnetization measurements were investigated with the SQUID magnetometer.

Experimental Section

Materials. The hybrid films were composed of a quaternary ammonium salt, didodecyldimethylammonium bromide (= DDAB) as the amphiphilic cation, montmorillonite (*Kunipia P*) as the clay mineral, and Co−Fe Prussian blue as the photomagnetic material. DDAB purchased from Aldrich was used as received and dissolved in chloroform to prepare a solution at 2.0×10^{-3} M.

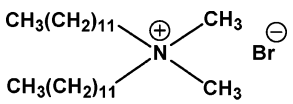

Structure of DDAB

The smectite clay mineral that we used (montmorillonite) was *Kunipia P* from Kunimine Co., Japan. The cation-exchange capacity (CEC) of the clay was 1.074 mequiv g^{-1}. The thickness of the clay single nanosheet, estimated from their crystal structure, was 9.6 Å.[23] The stock suspension of the clay was prepared by dispersing 1 g of the clay in 1000 mL of pure water and diluting it to a given concentration with pure water just before use as a subphase.

$CoCl_2$ and $K_3[Fe(CN)_6]$ were purchased from WAKO Pure Chemicals and used without further purification. The water was purified with a Simpli Lab water system (Millipore) to a specific resistivity of 18.2 MΩ cm.

Substrate Preparation. Glass plates were used as deposition substrates for X-ray diffraction (XRD) and X-ray photoelectron spectroscopy (XPS). A calcium fluoride (CaF_2) plate, purchased from Pier Optics Co., Ltd. (Japan), was used as a deposition substrate for the FT-IR measurements. Samples for SQUID measurement were prepared on Mylar (Teijin DuPont Films, Japan) substrates cleaned prior to use with absolute ethanol. All of the substrates were rendered hydrophobic by treating them with octadecyltriethoxysilane if needed.

Film Preparation. A schematic illustration of the film preparation process is shown in Figure 1. The solution of DDAB was spread on the subphase of the clay suspension (90 ppm) at room temperature. A floating monolayer of DDAB was hybridized with the clay single

(23) (a) Theng, B. K. G. *The Chemistry of Clay-Organic Reactions*; Adam Hilger: London, 1974. (b) Van Duffel, B.; Schoonheydt, R. A.; Grim, C. P. M.; De Schryber, F. C. *Langmuir* **1999**, *15*, 7520. (c) Moore, D. M.; Reynolds, R. C., Jr. *X-ray Diffraction and the Identification and Analysis of Clay Minerals*; Oxford University Press: New York, 1997.

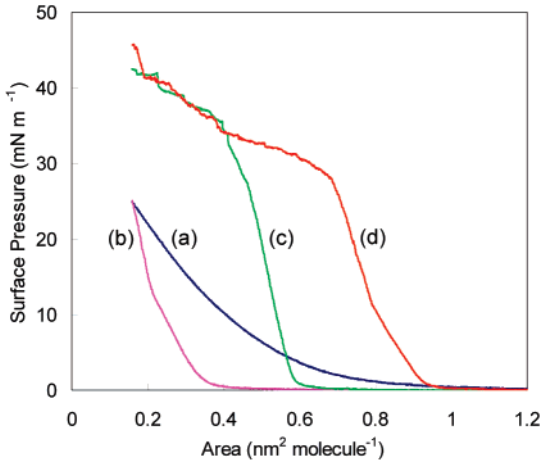

Figure 2. $\pi-A$ isotherm curves for floating monolayers of DDAB on (a) pure water and on the clay suspensions at (b) 20, (c) 40, and (d) 90 ppm.

nanosheet at the air−suspension interface. Fifteen minutes later, hybrid monolayers were compressed up to a surface pressure of 10 mN m^{-1}. After 30 min, floating hybrid monolayers were transferred as X-type films onto the hydrophobic surface of substrates by the horizontal dipping technique.[21b−d] The surface of the transferred film was rinsed with pure water several times and was then immersed in an aqueous $CoCl_2$ solution (10 mM) for 1 min to exchange the cobalt ions with the exchangeable metal ions. After rinsing the surface well with pure water again, it was dipped in an aqueous $K_3[Fe(CN)_6]$ solution (10 mM) for 1 min to form a Co−Fe Prussian blue layer on the surface of the hybrid film. The surface was rinsed well with pure water and dried by blasting with N_2. Hybrid films composed of DDAB, the clay single nanosheets, and Co−Fe Prussian blue were fabricated by repeating this procedure. One unit layer composed of DDAB, the clay single nanosheets, and Co−Fe Prussian blue is hereafter designated as one hybrid layer.

Instruments. The preparation of hybrid monolayers and measurements of the surface pressure−molecular area ($\pi-A$) isotherms were carried out using a computer-controlled film balance system, the FSD-50 (USI System, Japan). FT-IR absorption spectra were recorded on an FT-IR 660Plus spectrometer (JASCO, Japan). FT-IR measurements at low temperature were performed with a closed-cycle helium refrigerator (Iwatani Co., Ltd., Japan). Visible light illumination (400−700 nm, 1 mW cm^{-2}) was carried out using a xenon lamp (XFL-300, Yamashita Denso). XRD patterns were recorded on a Philips X'Pert MRD high-resolution X-ray diffractometer using Ni-filtered Cu Kα radiation. The XPS spectra were obtained on an ESCA Model 1600 C-type spectrometer (ULVAC-PHI, Inc., Japan) using the Al Kα line source at 1486.6 eV. Magnetic properties were investigated with a superconducting quantum interface device (SQUID) magnetometer (Model MPMS-5S, Quantum Design).

Results and Discussion

***π−A* Isotherms of Floating Hybrid Monolayers on Clay Suspensions.** Figure 2 shows the $\pi-A$ isotherms of hybrid monolayers when a solution of DDAB was spread onto the surface of the clay suspensions at 20, 40, and 90 ppm and also onto pure water.

The $\pi-A$ isotherm of DDAB floating monolayers on pure water (Figure 2a) shows the formation of a liquid expanded monolayer at the air−water interface. As already described in the literature,[24] this behavior is clearly due to the strong repulsion between polar head groups in the monolayer. When a clay suspension was used as the subphase, $\pi-A$ isotherms of DDAB were progressively modified. For example, the $\pi-A$ isotherm of hybrid monolayers on the clay suspension at 20 ppm (Figure 2b) lifted off at the smaller area (around 0.4 nm^2 molecule^{-1}) with a surface pressure of 0 mN m^{-1}, and as compressed, the surface pressure increased up to 25 mN m^{-1}. It appears that the lift-off area of the $\pi-A$ isotherms of the hybrid monolayers on the clay suspension (Figure 2, parts c and d) tends to shift toward larger areas as the concentration of the clay suspension increases. This trend indicates that charged DDAB monolayers could be electrostatically adsorbed onto the clay single nanosheets at the air−suspension interface.

This dependence on the isotherms has also been reported previously.[21,22] Briefly, the shift in the lift-off area on the isotherms is corresponding to changes in the density of amphiphiles at the air−suspension interface. In the case of this work, as already described above, the lift-off area on the isotherms shifted toward larger areas as the clay concentration in the suspension increases. In other words, it is supposed that the density of DDAB is small in hybrid monolyers prepared at higher clay concentration in the suspension. The lowering of DDAB density is caused by the fact that, due to the high clay concentration in the suspension, the hybrid monolayers are almost immediately formed at the air−suspension interface before DDAB themselves aggregate to form monolayer domains.

Structure of Hybrid Films. To determine the structure of the hybrid films, we performed XRD and XPS measurements. Samples for these measurements were prepared onto the glass substrate, and the layer number was 100 hybrid layers in both cases.

The presence of the cobalt and iron in the hybrid films is evidenced by XPS. The binding energies of each element were calibrated with the C (1s) peak of the hydrocarbon chain at 284.5 eV. In the XPS spectrum using the Al Kα line source (figure not shown), both Co (2p) and Fe (2p) peaks are found at 783.6 eV and 712.6 eV, respectively. The peak areas are integrated and corrected with atomic sensitivity factors[25] to yield the observed relative intensities for each element, and based on this calibration, a cobalt-to-iron ratio was calculated to be ca. 0.9. This ratio is an expected value when the cobalt ions and iron ions are reacting in the 1:1 stoichiometric manner to form Co−Fe Prussian blue. In this case, it is assumed that some alkali cations are incorporated into the interstitial position of the Co−Fe Prussian blue lattice to compensate the charge balance. Actually, this assumption is confirmed by the observation of the K (2p) peak at 305.0 eV. Moreover, in the spectrum, the peaks at 531.0, 402.0, and 284.5 eV were also found, which are assignable to O (1s), N (1s), and C (1s), respectively. The C (1s) and N (1s) peaks are from the CN group in Co−Fe Prussian blue and the DDAB molecules. With regard to the O (1s) peak, it is impossible to distinguish between the coordinated water molecules in the Co−Fe Prussian blue lattice and the oxygen atoms existing in the clay single nanosheets.

Next, we measured the XRD pattern in a $\theta-2\theta$ mode to confirm the layered structure of hybrid films. Figure 3 shows

(24) (a) Marra, J. *J. Phys. Chem.* **1986**, *90*, 2145. (b) Mingotaud, A. F.; Mingotaud, C.; Patterson, L. K. *Handbook of Monolayers*, 1st ed.; Academic Press: London, 1993; Vol. 1. (c) Clemente-León, M.; Agricole, B.; Mingotaud, C.; Gómez-García, C. J.; Coronado, E.; Delhaes, P. *Langmuir* **1997**, *13*, 2340. (d) Aiai, M.; Ramos, J.; Mingotaud, C.; Amiell, J.; Delhaes, P.; Jaiswal, A.; Singh, R. A.; Singh, B.; Singh, B. P. *Chem. Mater*. **1998**, *10*, 728.
(25) Wagner, C. D.; Davis, L. E.; Zeller, M. V.; Taylor, J. A.; Raymond, R. M.; Gale, L. H. *Surf. Interface Anal*. **1981**, *3*, 211.

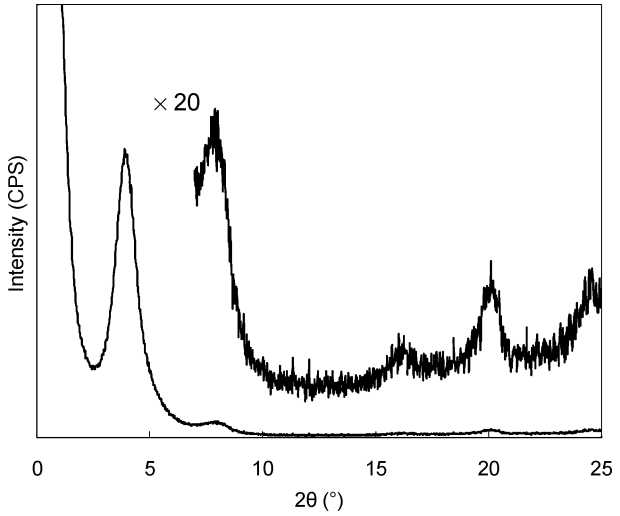

Figure 3. XRD patterns for a 100-layered hybrid film (DDAB/clay single nanosheets/Co−Fe Prussian blue).

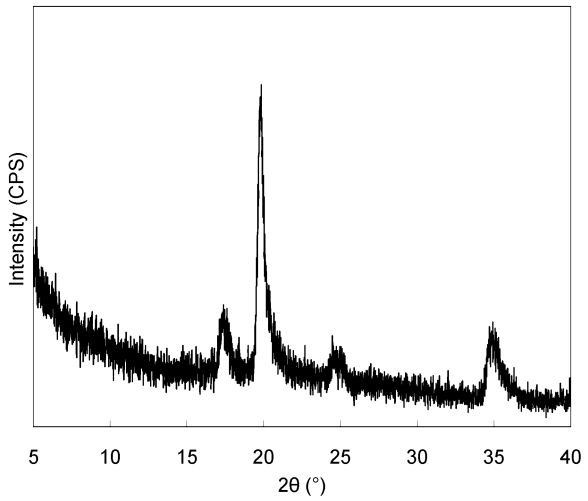

Figure 4. In-plane XRD patterns for a 100-layered hybrid film (DDAB/clay single nanosheets/Co−Fe Prussian blue).

the XRD pattern of the films, and as can be seen, five diffraction peaks were given at $2\theta = 3.94$, 7.87, 16.1, 19.9, and 24.5°.

These peaks are ascribed to the (001), (002), (004), (005), and (006) reflections of the clay layer, respectively.[23] Thus, hybrid films obviously possess the layered structure, and from the (001) diffraction peak, the basal spacing of the unit layer (DDAB/clay single nanosheets/Co−Fe Prussian blue) is calculated to be 22.4 Å. According to our previous photomagnetic LB films,[22c] which were composed of an amphiphilic azobenzene, clay minerals, and Prussian blue, alkyl chains of the amphiphile are almost perpendicular to the film surface. Therefore, also in the present system, it is supposed that alkyl chains of DDAB are almost perpendicular to the film surface. Taking this estimation into account, the thickness of the adsorbed Co−Fe Prussian blue layers (−NC−Fe−CN−Co−O) is calculated to be 4.0 Å. In this case, also similar to our previous system,[22c] roughly a single layer (half of the unit cell) of the Co−Fe Prussian blue network would be formed in the hybrid films.

As mentioned above, it is confirmed that the hybrid films possess the layered structure. Subsequently, an in-plane XRD measurement was performed in order to verify the presence of in-plane structural correlations in the films. As a result, four diffraction peaks were given at $2\theta = 17.6$, 19.8, 25.1, and 35.0° (Figure 4).

Peaks at $2\theta = 17.4$ and 25.1° are corresponding to the (200) and (220) Bragg reflections at *d*-spacings of 5.10 and 3.55 Å, respectively, from a face-centered square cell of $a = 10.2$ Å for the Co−Fe Prussian blue structure,[26] and those at $2\theta = 19.8$ and 35.0° are assignable to the (110), (020), and (130) reflections of the clay layer.[27] From this result, it is indicated that the adsorbed Co−Fe Prussian blue layer forms the ordered structure along the film surface plane. That is, the structure of the Co−Fe Prussian blue layer would be a two-dimensional network, and moreover, analysis of the (200) peak width by application of the Scherrer equation[28] yields an average crystalline coherence length of ∼160 Å, or a 16 unit cell length. Recently, Culp et al. have reported that the two-dimensional grid network of Prussian blue analogues could be successfully formed by using the air−water interface.[18] Although their LB system is quite sophisticated, it is required to choose the appropriate amphiphiles and the subphase. However, in our hybrid system reported herein, there is little constraint in the choice of components compared with their work. Actually, we have recently demonstrated that it is enabled to realize the two-dimensional ordering of the metal complex by utilizing this method.[27b]

FT-IR Absorption Spectra of Hybrid Films. The formation of hybrid films was monitored by FT-IR absorption spectra measured in the process of the film preparation at room temperature. Each spectrum gave some characteristic stretching vibration bands (figure not shown): CH_3 antisymmetric (at 2957 cm^{-1}), CH_2 antisymmetric (at 2925 cm^{-1}) and symmetric (at 2848 cm^{-1}), and CN bridging (at 2159 cm^{-1}, $Fe^{III}-CN-Co^{II}$, and at 2094 cm^{-1}, $Fe^{II}-CN-Co^{II}$). To confirm a reproducible transfer of hybrid monolayers, the absorbance of the CH_2 antisymmetric and symmetric vibration was plotted as a function of the layer number, respectively (Figure 5).

Each absorbance increased regularly as the layer number increased. Therefore, the transfer of hybrid monolayers proceeded successfully. Similarly, successive formation of Co−Fe Prussian blue onto the clay layer was monitored by plotting the absorbance of the CN stretching vibration versus layer number (Figure 6).

As a result, a regular increase in absorbance was also seen, and hence, the adsorption process of Co−Fe PB was also reproducible.

After hybrid films (100 hybrid layers) were fabricated, the FT-IR absorption spectrum was also measured at low temperature (8 K). The result (only the region of the CN stretching vibration) is shown in Figure 7, with a comparison of the spectrum measured at room temperature (300 K).

As can be seen, two absorption peaks were found in each spectrum. When the spectrum was measured at 300 K, the peaks are located at 2159 and 2094 cm^{-1}. Besides, measured at 8 K,

(26) (a) Buser, H. J.; Schwarzenbach, D.; Petter, W.; Ludi, A. *Inorg. Chem.* **1977**, *16*, 2704. (b) Herren, F.; Fischer, P.; Ludi, A.; Hälg, W. *Inorg. Chem.* **1980**, *19*, 956. (c) Yamada, S.; Kuwabara, K.; Koumoto, K. *Mater. Sci. Eng., B* **1997**, *49*, 89.

(27) (a) Takahashi, S.; Taniguchi, M.; Omote, K.; Wakabayashi, N.; Tanaka, R.; Yamagishi, A. *Chem. Phys. Lett.* **2002**, *352*, 213. (b) Umemura, Y.; Shinohara, E. *Chem. Commun.* **2004**, 1110.

(28) Guinier, A. *X-ray Diffraction*; Freeman: San Francisco, CA, 1968.

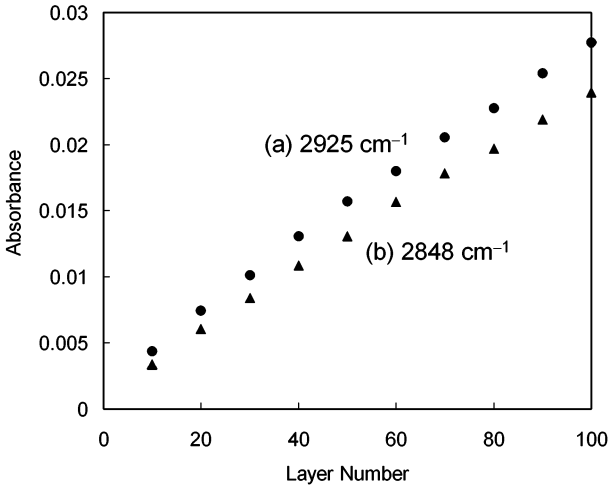

Figure 5. Changes in absorbance at (a) $\nu = 2925$ cm^{-1} (filled circles) and (b) $\nu = 2848$ cm^{-1} (filled triangles) against the number of hybrid layers. Background subtraction was done for both data.

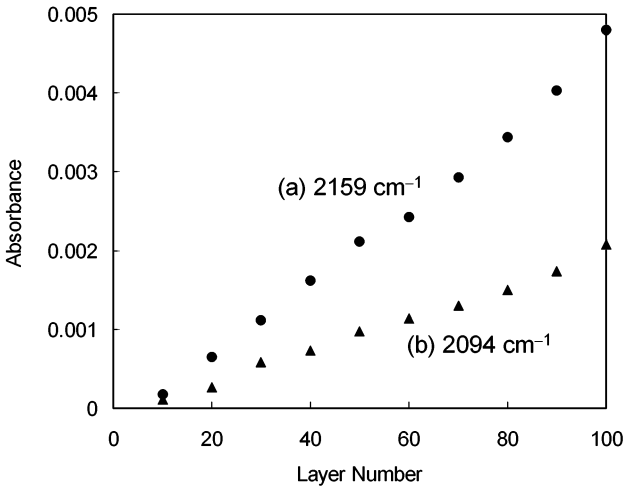

Figure 6. Changes in absorbance at (a) $\nu = 2159$ cm^{-1} (filled circles) and (b) $\nu = 2094$ cm^{-1} (filled triangles) against the number of hybrid layers. Background subtraction was done for both data.

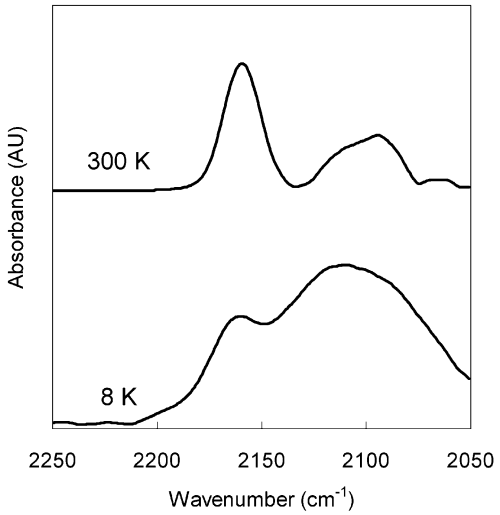

Figure 7. FT-IR spectra for a 100-layered hybrid film measured at (a) RT (300 K) and (b) 8 K.

the peak at 2159 cm^{-1} remained; however, the peak at 2094 cm^{-1} became broadened and the absorption maximum shifted toward higher wavenumber, centered at 2112 cm^{-1}. The observation of such a temperature dependence in the FT-IR absorption spectrum has been reported.[5b,e] In each reported case, the position of the CN stretching vibration band is affected by the chemical composition of the Co−Fe Prussian blue. In other words, it depends on the valence state of the cobalt and iron ions in the Co−Fe Prussian blue lattice. Therefore, it is possible to deduce the valence state of metal ions from the FT-IR absorption spectrum. In our system, according to this information, it is able to determine the valence state of Co−Fe Prussian blue in hybrid films. At 300 K, the observed peaks at 2159 and 2094 cm^{-1} are assignable to the stretching of the CN bridge with the Fe^{III}−CN−Co^{II} and Fe^{II}−CN−Co^{II} bond structures, respectively. In addition, at 8 K, the broadened peak centered at 2112 cm^{-1} is ascribed to the Fe^{II}−CN−Co^{III} moiety. As already mentioned, this peak shifted toward higher wavenumber by 18 cm^{-1} compared with that assigned to the Fe^{II}−CN−Co^{II} one. This shift is due to the change in the electronic states of cobalt ions from high-spin Co^{II} (HS, $S = {}^3/_2$) to low-spin Co^{III} (LS, $S = 0$), where HS and LS represent high-spin and low-spin, respectively.[5b,e] Here, the decrease of the e_g electrons with antibonding character leads to the increase in back-bonding accompanied by a partial depopulation of the π^*(N−C) orbital in order to compensate the charge deficit at the central ion caused by the back-bonding. The decrease of the electrons in antibonding π^*(N−C) results in the shift of the ν (CN) value toward higher wavenumber. Moreover, upon cooling from 300 to 8 K, the electronic state of the cobalt ions changed (i.e., from high-spin to low-spin). According to previous reports,[5c−e] such a spin transition in Co−Fe Prussian blue occurs when some alkali cations are incorporated into the lattice. Therefore, in our case, the observation of the spin transition indicates that alkali cations exist in the interstitial sites of Co−Fe Prussian blue. The result of the XPS also supports the presence of alkali cations (K^+) in the lattice.

Photoinduced Electron Transfer in Hybrid Films at Low Temperature and Its Relaxation Process. As first reported by Sato et al.,[5a] upon red light illumination, the electron transfer from Fe^{II} to Co^{III} through the CN group occurred at low temperature. As a result, the oxidation state changed into Fe^{III}-(LS, $S = {}^1/_2$)−CN−Co^{II}(HS, $S = {}^3/_2$) from Fe^{II}(LS, $S = 0$)−CN−Co^{III}(LS, $S = 0$). This photoinduced electron-transfer process has been mostly discussed by monitoring changes in the FT-IR absorption spectra (CN bridging mode) at low temperature.

As mentioned above, Figure 7 compares the results of FT-IR absorption spectra measured at 300 and 8 K. As can be seen in the figure, most cobalt ions exist as the high-spin state at 300 K: the main absorption peak is located at 2094 cm^{-1}. On the contrary, at 8 K, the spin state of the cobalt ions changes into low-spin: the peak broadened and its center shifted to 2112 cm^{-1}. Subsequently, we examined the photoinduced electron transfer upon illuminating with visible light, and the result is shown in Figure 8.

Before illumination, as already described, the broad peak centered at 2112 cm^{-1} was observed. This peak was ascribed to the CN stretching vibration Fe^{II}(LS, $S = 0$)−CN−Co^{III}(LS, $S = 0$). Upon visible light illumination, the peak separated into the two peaks located at 2163 and 2092 cm^{-1}, attributed to the CN bridging mode of Fe^{III}(LS, $S = {}^1/_2$)−CN−Co^{II}(HS, $S = {}^3/_2$) and Fe^{II}(LS, $S = 0$)−CN−Co^{III}(LS, $S = 0$), respectively.

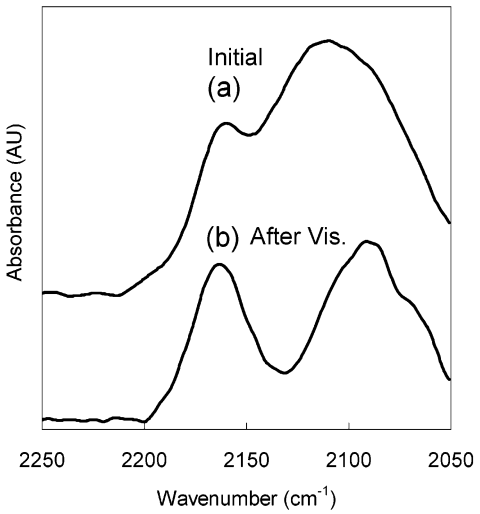

Figure 8. FT-IR spectra for a 100-layered hybrid film measured at 8 K: (a) initial state and (b) after visible light illumination at 8 K.

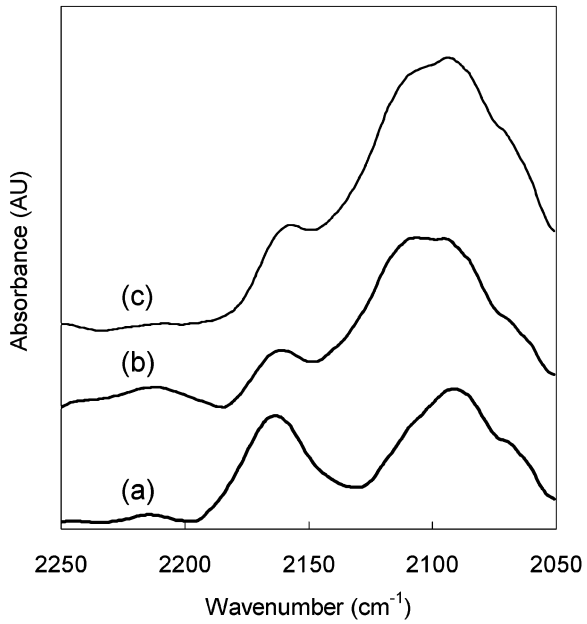

Figure 9. Temperature dependence of FT-IR spectra for a 100-layered hybrid film after visible light illumination at 8 K: (a) 8 K, (b) 160 K, and (c) 300 K.

The longer the illumination time was, the more the reaction proceeded.

It has been reported that the generated high-spin state relaxed into the initial state (low-spin state) by annealing above 150 K.[5b] To confirm the relaxation temperature, we measured the temperature dependence of the FT-IR absorption spectrum (Figure 9).

Upon heating, the peak at 2163 cm^{-1} decreased, and in contrast, the peak at 2092 cm^{-1} increased. As the temperature reached 160 K, the peak at 2092 cm^{-1} shifted toward higher wavenumber and broadened (Figure 9b). In other words, the CN bridging mode returned to its initial state: Fe^{II}(LS, $S = 0$)−CN−Co^{III}(LS, $S = 0$). It was also observed that further heating led to the enhancement of this peak. In this sense, the electron transfer from the Co^{II}(HS, $S = {}^3/_2$) species back to the Fe^{III}(LS, $S = {}^1/_2$) one is thermally induced.

Magnetic Properties of Hybrid Films. Magnetic properties were investigated with the SQUID magnetometer. First, we measured the FCM curves (with an applied magnetic field of 10 G) for hybrid films to confirm the magnetic interactions in the films (Figure 10).

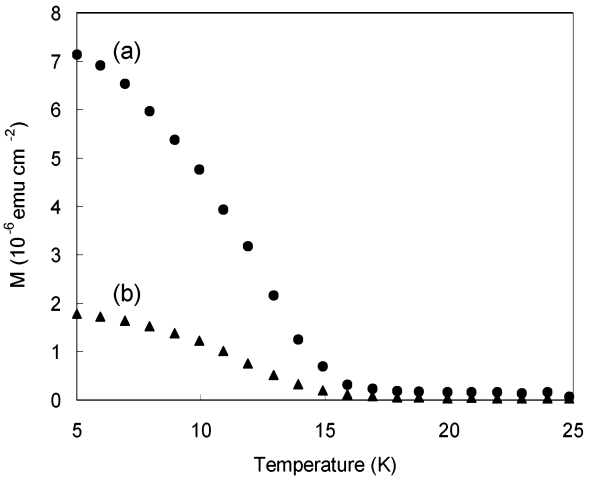

Figure 10. Temperature dependence of the magnetization for a 100-layered hybrid film after field cooling in 10 G: (a) the sample surface aligned parallel to the applied magnetic field and (b) the sample surface aligned perpendicular to the magnetic field.

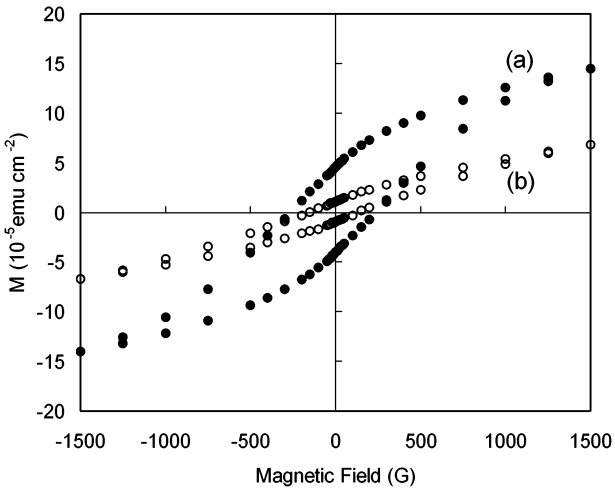

Figure 11. Hysteresis loops for a 100-layered hybrid film measured at 5 K: (a) the sample surface aligned parallel to the applied magnetic field and (b) the sample surface aligned perpendicular to the magnetic field.

Thus, hybrid films clearly exhibited the magnetic anisotropy due to the low-dimensional structure of the Co−Fe Prussian blue layer. In detail, when the film surface was oriented parallel to the applied magnetic field, the observed magnetization values were higher than the film surface oriented perpendicular to the magnetic field. That is, the magnetic easy axis lies along the film surface plane and the magnetic hard axis along the plane perpendicular to the surface. In both orientations, the rise in the magnetization was observed below $T_c = 14$ K, which indicates the onset of the long-range ferrimagnetic order. The presence of a ferrimagnetic state at low temperature is further supported by the dependence of the magnetization on the applied magnetic field data taken at 5 K. The sample showed a rapid increase in the magnetization at low field followed by a gradual approach toward saturation at higher fields. Cycling the magnetic field at 5 K resulted in the hysteresis loops (Figure 11).

Again, there is clear anisotropy in the magnetic behavior between the two orientations of the sample with regard to the

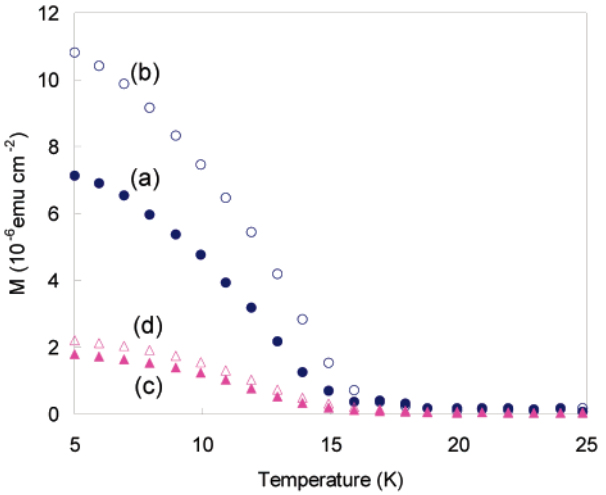

Figure 12. Temperature dependence of the magnetization for a 100-layered hybrid film before and after visible light illumination at 5 K: (a) initial state in parallel orientation to the magnetic field, (b) photoinduced state in parallel orientation to the magnetic field, (c) initial state in perpendicular orientation to the magnetic field, and (d) photoinduced state in perpendicular orientation to the magnetic field.

magnetic field. When the magnetic field is parallel to the sample surface (Figure 11a), the magnetization increases more rapidly with respect to the field and the remnant magnetization is 31% versus 14% in the perpendicular orientation (Figure 11b). The coercive field is also slightly anisotropic, being 250 G in the parallel orientation and 150 G in the perpendicular orientation.

Subsequently, we investigated the photoinduced magnetization effect of the Co−Fe Prussian blue in the hybrid films. Light illumination was performed at 5 K with an applied magnetic field of 10 G, and the wavelength range of the light was 400−700 nm. The influence on the magnetization upon light illumination was examined in both orientations with regard to the applied magnetic field (the parallel and perpendicular orientation). Figure 12 demonstrates the results in changes in the magnetization upon light illumination.

As seen in the figure, the photoinduced magnetization effect was observed in both orientations (Figure 12, a to b and c to d). However, the degree of increase in the magnetization was different in the direction of the applied magnetic field. In this sense, interestingly, the photoinduced magnetization effect was also anisotropic. The magnetization increase is much more intense when the magnetic field is parallel to the sample surface, and the changes in the magnetization are 60% versus 10% in the perpendicular orientation.

As briefly mentioned in the Introduction, Park et al. recently reported an anisotropic photoinduced magnetism in Co−Fe Prussian blue thin films prepared by the sequential assembly method.[20d] According to their results, upon light illumination at 5 K, the net magnetization of the film increased when the surface of the film was oriented parallel to the external magnetic field. On the other hand, when the surface of the film was perpendicular to the magnetic field, the net magnetization decreased upon illumination. They describe that the anisotropic photoinduced magnetization effect in the film arises from the interplay between the low-dimensional nature of the system and the dipolar magnetic fields generated by the ferrimagnetic domain. Before light illumination, the net magnetic field is the vector sum of the external magnetic field (H_E) and the dipolar field (H_D) in which H_D is antiparallel to H_E, and after light illumination, the direction of the photoinduced magnetization will follow that of the net magnetization. Along this line, the net magnetization of the film in the photoinduced state decreases when $H_D > H_E$ in the case of the film surface oriented perpendicular to H_E. On the contrary, when the film surface was oriented parallel to the H_E, due to the two-dimensional nature of the film, the diamagnetic sites undergo a net magnetic field which is always in the direction of H_E, and hence, the photoinduced diamagnetic to ferrimagnetic conversion results in a global increase in the total magnetization.

Our observed anisotropic behavior in the photoinduced magnetization was not consistent with the results derived from Park et al. that have already been mentioned above. It is supposed that this difference is mainly due to the structure of the Co−Fe Prussian blue in the films: the layer thickness, the in-plane structural coherence length, and the structure of Co−Fe Prussian blue network. In our system, with respect to the layer thickness, the Co−Fe Prussian blue layers are well isolated from each other by DDAB and the clay layer. Moreover, according to the XRD measurement, Co−Fe Prussian blue forms the single-layered structure (thickness ∼4.0 Å), and the structural coherence length was estimated to be ∼160 Å from the in-plane XRD measurement. On the other hand, in the system of Park et al., the Co−Fe Prussian blue film is built up by the sequential assembly method and has an average thickness of about 2000 Å. In this sense, the Co−Fe Prussian blue network is well developed in the perpendicular direction to the film surface. Although the in-plane structural coherence length of the Co−Fe Prussian blue in the film was not given in their literature, it is deduced to be close to our estimated value, according to their previous work.[29] Therefore, in-plane structural coherence would not be related to the difference in the anisotropic behavior of the photoinduced magnetization effect. However, one possibility occurs to explain our observed anisotropic photoinduced magnetization effect. That is, the structure of the Co−Fe

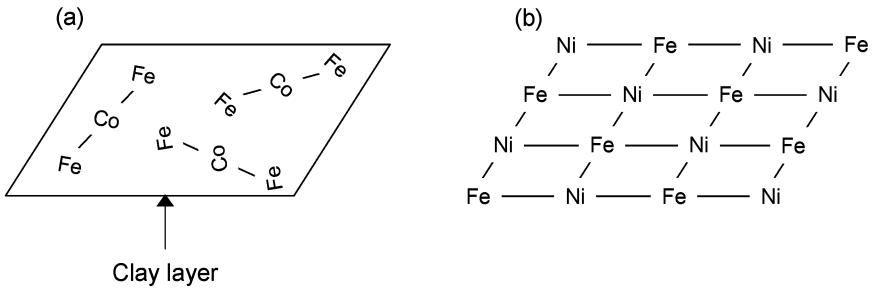

Figure 13. Simple illustration of the Co−Fe Prussian blue network in hybrid films: (a) our system and (b) the "perfect" two-dimensional grid system (ref 18). In this illustration, CN bridging ligands are omitted for clarity (denoted as a line).

Prussian blue network onto the clay layer would be disordered to some extent. In detail, Co−Fe Prussian blue does not form a "perfect" two-dimensional grid network. Figure 13 illustrates the deduced structure of the Co−Fe Prussian blue in our film, with a comparison to the system fabricated by Culp et al. that demonstrates the successful formation of the "perfect" two-dimensional grid network of Prussian blue analogues (Ni−Fe Prussian blue).[18]

As can be seen in the figure, in our film, the coherent Co−Fe Prussian blue network would not be linked and separated from each other. In other words, each network forms an isolated wire- or rodlike structure. Actually in the FT-IR spectra, the frequencies of the CN stretching vibration (bridge mode) shifted to some extent (10−20 nm), probably because the local symmetry of the ions was reduced in such a manner. In this case, the generated dipolar field would be minimized, and hence, the net magnetic field acting on the Co−Fe Prussian blue is nearly equal to the applied magnetic field. Therefore, despite the generation of high-spin species by the photoinduced electron transfer from Fe^{II} to Co^{III}, the resultant increase of the spin values was not reflected to the magnetization values due to the existence of magnetic anisotropy in the film. As a result, the degree of the photoinduced magnetization is consistence with that of the magnetization before light illumination.

(29) They have prepared the Prussian blue (also its analogue) thin film by the same sequential assembly method. According to the grazing incidence X-ray diffraction (GIXD) measurements, the coherence length was calculated to be 190 and 150 Å for the Prussian blue and Ni−Cr Prussian blue films, respectively. See details in their previous report in ref 20.

Conclusions

We have prepared thin films of Co−Fe Prussian blue by means of the modified LB method using a clay mineral. In this method, hybrid LB films composed of DDAB and montmorillonite play a template role for the formation of the Co−Fe Prussian blue layer. The hybrid films possess well-organized structure and exhibit magnetic anisotropy due to the unique nature of Co−Fe Prussian blue. Moreover, its photoinduced magnetization effect was also anisotropic. The present work demonstrates that the clever use of an air−liquid interface can be quite effective for designing and fabricating magnetic thin films. In addition, this work may offer new perspectives, not only for nanoscale composite materials but also for understanding the magnetic interaction in low-dimensional systems.

Acknowledgment. This work was supported by a Grant-in-Aid for Scientific Research on Priority Area (417) and the 21st Century COE program "KEIO Life Conjugate Chemistry" from the Ministry of Education, Culture, Sports, Science, and Technology (MEXT) of the Japanese Government.

Supporting Information Available: XPS spectra, changes in FT-IR spectra, and plots of the amount of high-spin species against the visible light illumination time for a 100-layered hybrid film. This material is available free of charge via the Internet at http://pubs.acs.org.

JA053131E

Supporting Information

for

"Observation of the Anisotropic Photoinduced Magnetization Effect in Co–Fe Prussian Blue Thin Films Fabricated by Using the Clay Langmuir–Blodgett Films as a Template."

Takashi Yamamoto[†], *Yasushi Umemura*[‡], *Osamu Sato*[§], *and Yasuaki Einaga*[†*]

† Department of Chemistry, Faculty of Science and Technology, Keio University,

3-14-1 Hiyoshi, Yokohama 223-8522, Japan

‡ Department of Applied Chemistry, National Defense Academy,

1-10-20 Hashirimizu, Yokosuka 239-8686, Japan

§ Department of Molecular and Material Sciences, Interdisciplinary Graduate School of Engineering Sciences, Kyushu University,

6-1 Kasuga-koen, Kasuga 816-0811, Japan

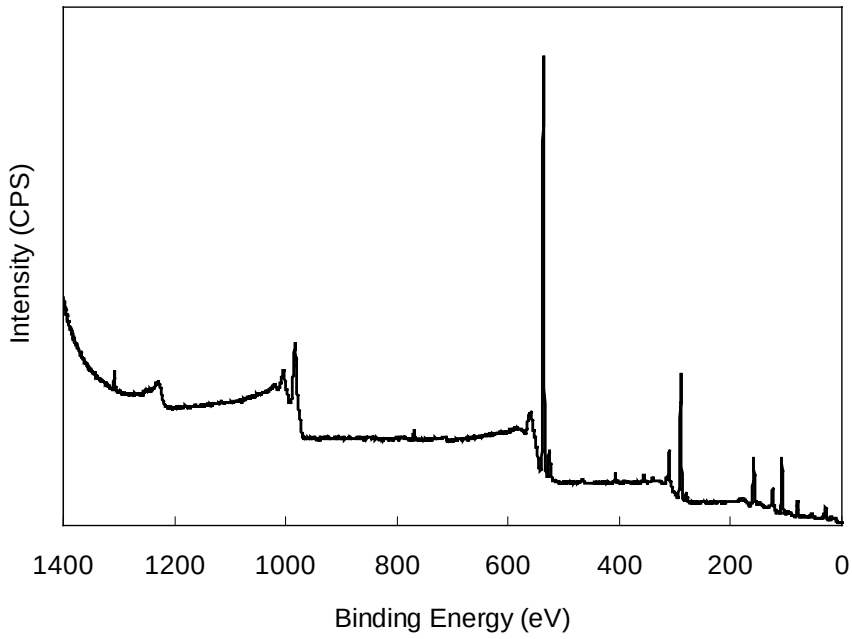

Figure S1. XPS survey spectrum of for a 100-layered hybrid film.

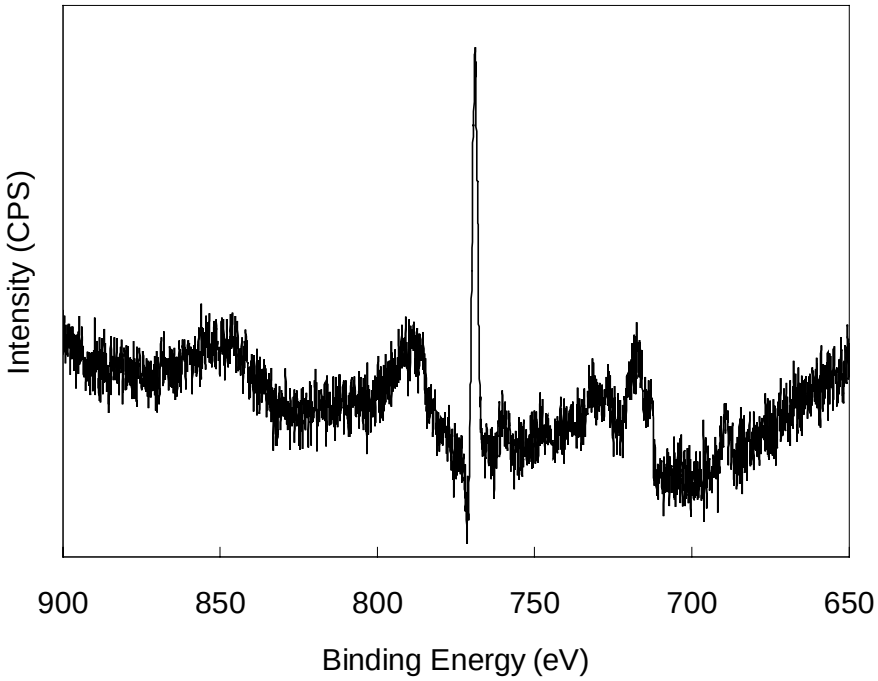

Figure S2. XPS multiplex spectrum of for a 100-layered hybrid film.

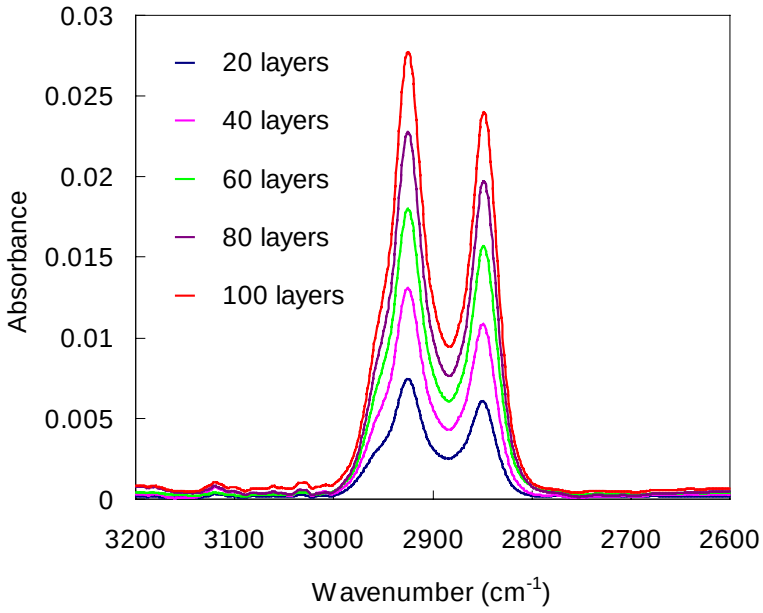

Figure S3. Changes in the FT–IR spectra (CH_2 stretching vibration region) during the film preparation process.

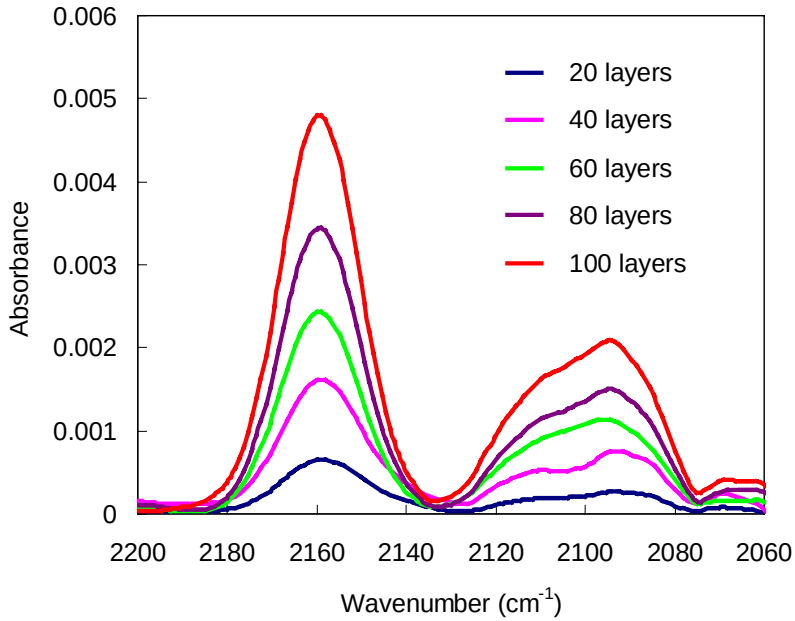

Figure S4. Changes in the FT–IR spectra (CN stretching vibration region) during the film preparation process.

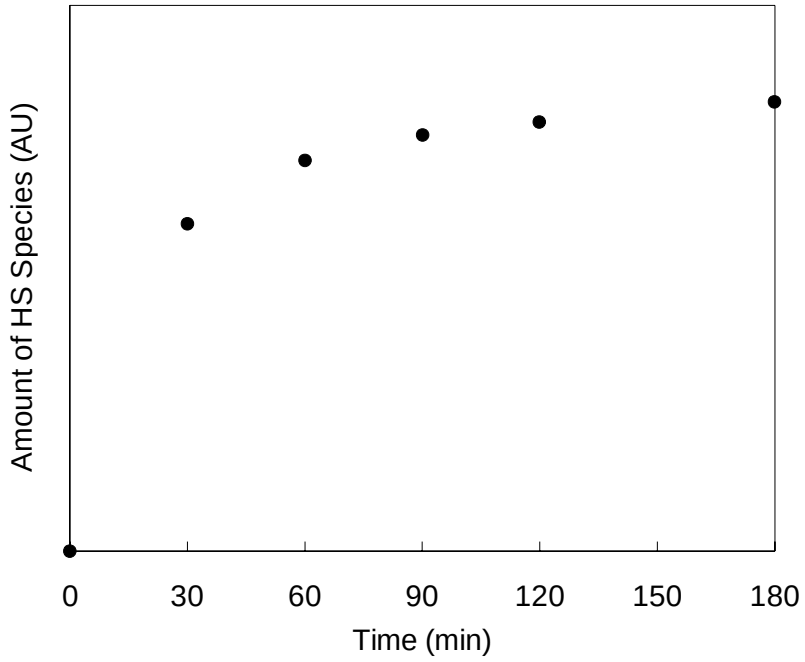

Figure S5. Plots of the amount of HS (high-spin) species against the visible light illumination time for a 100-layered hybrid film. In this figure, the amount of HS species are estimated from the ratio of peak intensity, *I* (2163 cm^{-1}) / *I* (2112 cm^{-1}), in the FT-IR spectra measured at 8 K. Although there exist the HS (high-spin) species before illumination, normalization of the ratio in the initial state is adopted so that it is easy and helpful to understand the photoinduced changes.